# Surface Potential Based Compact I-V Model for GaN HEMT Devices

Chenfei Chang, Jin He, Chunlai Li, Yandong He, Jingjing Liu, Xiaomeng He, Jun Pan, Guoqing Hu, and Yuan Ren

SoC Key Laboratory, Peking University Shenzhen Institute and PKU-HKUST Shenzhen-Hong Kong Institution

## ABSTRACT

Gallium Nitride (GaN)-based high electron mobility transistors (HEMTs) are emerging as promising contenders to replace existing Silicon and Gallium Arsenide (GaAs) devices in the radio-frequency/microwave power amplifiers and high-power switching applications. Along with the fast development of device technology and circuit integration, compact models for GaN HEMTs are of great value for circuit design and simulation. In this paper, an analytical drain current model for GaN HEMTs is developed based on the definition of surface potential. The electrostatic potential solution is provided first by solving the charge control equations. Based on the surface potential model, a close formed and SPICE friendly drain current model is developed for GaN HEMTs which captures the core physics and some additional effects in HEMT devices. Then, the model is calibrated and validated with TCAD simulations, and the experimental I-V measurements of fabricated devices.

**Keywords:** GaN- HEMTs, compact model, device physics, SPICE, circuit simulation, RF and power application.

## 1 INTRODUCTION

The GaN material has overall advantages comparing to the other semiconductor materials in the application area of power amplifier/switching technologies, in comparison between SiC, Si, GaAs, InP and GaN from the basic material properties that are most important to electronic device performance [1-7]. As a kind of wide bandgap (WBG) material, GaN allows high electric breakdown fields and high operating temperatures. GaN has a relatively low electron mobility compared to GaAs and InP. However, the electron mobility $\mu_n$ and saturation velocity $v_{sat}$ of the two dimensional electron gas (2DEG) at the AlGaN/GaN heterojunction is very suitable for high-power and high-frequency device applications. The 2DEG sheet charge density ($n_s$) due to piezoelectric and spontaneous polarization effect is one order higher than those of other heterojunctions, which also promises the extremely high power density of GaN power devices. For the thermal conductivity ($\kappa$) which determines the degradation of device performances at elevated temperatures, GaN is comparable with Si and better than GaAs and InP. These above-mentioned competitive advantages of the GaN material for both military and commercial applications attract the interest from both the researchers and industries in the recent years.

With the device technology getting mature and the market increasing, the physics based analytic model will dominate the model development. Currently, there are two major kinds of physical models for GaN HEMTs: the threshold voltage ($V_{th}$)-based model and surface potential based model. In the first several years of the 20th century, the Vth-based model was developed for GaN HEMTs [8-11]. However, the smooth functions to transit different regions are missing, thus it cannot satisfy the continuity issue in the SPICE simulations. With the higher requirement on the continuity and symmetry of the model in recent years, people began to develop the surface potential based model [12-20]. However, the model followed the same way as for MOSFET to construct the surface potential equations, and did not consider the quantum effect which is very important for GaN HEMTs. Therefore, the model is not that accurate for GaN-based devices. Later in 2011, the Tsinghua group published their work on the surface potential-based current model with a new definition to the surface potential which is more adaptable for GaN HEMTs [12-13], and the quantum effect is considered when calculating the channel 2DEG density.

This paper is devoted to developing the surface potential based DC I-V model for GaN HEMTs with a number of enhanced features to an engineering model which is suitable for circuit simulations based on the definition of surface potential. The electrostatic potential solution is provided first by solving the charge control equations. Based on the surface potential model, a close formed and SPICE friendly drain current model is developed for GaN HEMTs which captures the core physics and some additional effects in HEMT devices.

## 2 MODEL DEVELOPMENT

### 2.1 Generic Structure of GaN HEMTs

Fig. 1 is the Cross-sectional schematic of a typical GaN HEMT. The region in red box is the core region of the device and those in yellow boxes are the access regions. The GaN buffer layer is the location of the channel 2DEG. Even though the 2DEG is located mainly in the surface 10-nm-depth region under the heterojunction, the thickness of this layer is about 2 μm. This is for improving the surface quality of the GaN layer and increasing the insulation ability besides the substrate layer. To reduce to the scattering effect, the GaN layer is typically undoped, but usually it will be unintentional doped as n-type and acceptor-type traps will be induced in this layer. The AlGaN layer forms an energy well with the GaN layer.

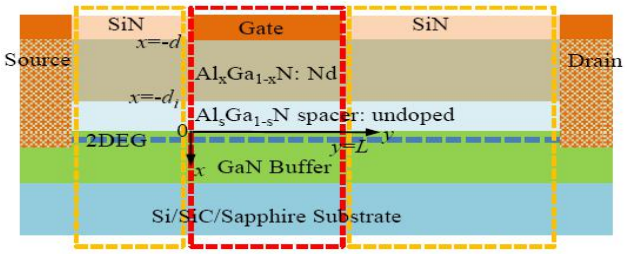


Fig.1 Cross-sectional schematic of a typical GaN HEMT.

For the compact model development of HMET devices, more attention pays on the functional core region, which is the gated region in red box in Fig. 1, and the other parts are considered as additional resistances to form a full model, and the internal nodes are used in this process. In this paper, the same flow is followed by modeling the core region first and then using internal nodes to incorporate the access region resistances. Here, all symbols have the common physics meanings as shown in the tab le I.

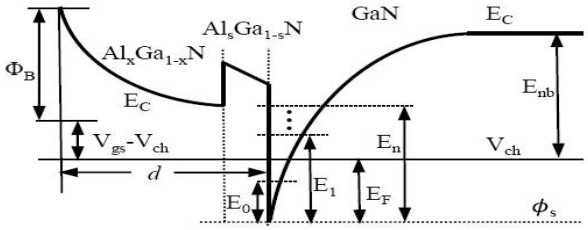


Fig. 2 Energy band diagram of a GaN HEMT for $V_{gs}$.

Table I Symbols definition for surface potential solution.

| Symbols | Definitions |
|---|---|
| $n_s$ | The sheet charge density (density of 2DEG) |
| $V_{OFF}$ | The offset voltage |
| $V_{ch}$ | The channel potential |
| $\varepsilon_{AlGaN}$ | The permittivity of AlGaN layer |
| $d_d$ | The thickness of the doped AlGaN layer |
| $d_i$ | The thickness of the AlGaN spacer layer |
| $d$ | The thickness of the AlGaN layer, $d=d_d+d_i$ |
| $q$ | The electron charge |
| $\phi_s$ | The surface potential |
| $E_F$ | The Fermi level relative to the bottom of the conduction band |
| $E_i$ | The subband levels relative to the bottom of the conduction band |
| $u_i$ | Position of $E_i$ determined by Robin boundary condition |
| $D$ | The conduction band density of states of a 2D system |
| $k$ | The Boltzmann's constant |
| $T$ | The ambient temperature |
| $\phi_t$ | The thermal voltage, $\phi_t = kT/q$ |

## 2.2 Surface potential modeling

The current and charge characteristics are dependent on the channel charge density, which can be derived from the energy band distribution. For the GaN HEMT structure shown as Fig. 1 where the three-dimensional effects are neglected, the conduction band diagram is given in Fig. 2. In the defined HEMT structure in Fig.1, the all symbols have the common physical meaning, and the origin of coordinates is at the source side gate edge of the heterojunction. To develop a surface potential based model, the definition of surface potential is necessary. To simplify expressions of the charge density, the surface potential in this study is defined as the bottom of conduction band relative to the channel potential as shown

$$\phi_s = V_{ch} + E_F \qquad (1)$$

The well-known charge control equations [12] as self-consistent solution of Poisson's equation and Schrodinger's equations in the quantum well , are expressed as:

$$n_s = \frac{\varepsilon_{AlGaN}}{qd}(V_{gs} - V_{ch} - V_{OFF} - E_F) = \frac{\varepsilon_{AlGaN}}{qd}(V_{gs} - V_{OFF} - \phi_s) \qquad (2)$$

$$E_i = -u_i(0)\left(\frac{\hbar^2 q}{2m^*\varepsilon_{GaN}^2}\right)^{\frac{1}{3}} n_s^{\frac{2}{3}} = u_i n_s^{\frac{2}{3}} \qquad (3)$$

$n_s$ prediction as other complex functions as shown

$$n_s = \sum_{i=0}^{\infty} DkT \ln\left[1 + \exp\left(\frac{E_F - E_i}{\phi_t}\right)\right] \qquad (4)$$

where the dielectric constant of AlGaN layer is

$$\varepsilon_{AlGaN} = d\varepsilon_i\varepsilon_d / (d_d\varepsilon_i + d_i\varepsilon_d) \qquad (5)$$

$V_{OFF}$, which is the offset voltage similar as the flatband voltage in MOSFETs, is given as

$$V_{OFF} = \Phi_B - (\Delta E_{C1} + \Delta E_{C2}) - \frac{qN_d d_d^2}{2\varepsilon_x} - \frac{q\sigma_x d}{\varepsilon_x} \qquad (6)$$

It is impossible to calculate all the energy subbands while it is also unnecessary since the electrons are mainly distributed in the lower subbands. To improve calculation efficiency, only the zero subband energy level $E_0$ is considered to solve the channel charge since the electrons contributed by other subbands can be neglected in the valid regions. In this study, the surface potential calculation follows the three-order correction method referring to the silicon-based surface potential modelling [19]. The key of this method is to give an initial solution first and then use a correction term to refine it. After two or three time refinements, the absolute error of the $E_F$ can reach a very low level which is necessary for the precise calculation of charges and currents.

Fig.3 shows the comparison between the model with three time refinements and the numerical solutions which also only consider E0. The absolute error of the $E_F$ reaches under 10fV with extensive validations by changing the AlGaN layer thickness and the operation temperature. This excellent agreement promises the feasibility of surface potential based current and terminal charge model which requires precise surface potential solutions for the model accuracy.

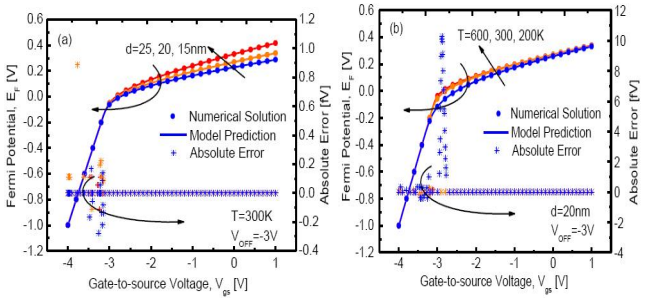


Fig.3 Comparison between the numerical solution and model prediction and the absolute error by changing (a) the thickness of AlGaN layer d and (b) the temperature T.

Fig.4 compares the model prediction charge-sheet density with the TCAD simulations and the numerical results with changing the AlN mole fraction x and the thickness of the AlGaN layer thickness [20]. The Schottky gate barrier height is set as 1.5eV. The numerical results are obtained by solving (1-4) iteratively which only consider $E_0$. Good agreements are achieved, which promises the feasibility of current and terminal charge models.

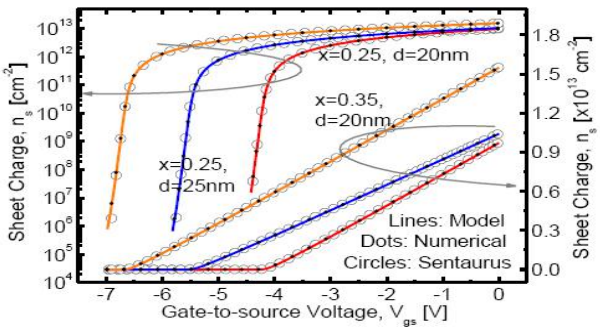


Fig.4 Comparison of analytical models, TCAD simulations and numerical results of sheet charge density.

### 2.3 Drain current modeling

Based on the precise solution of surface potential, the drain current model is developed. The mobility model and the channel length modulation effect are included in the model. Some unique phenomenon like the self-heating effect and the field plate structures are also incorporated.

The normalized channel electron density is written as:

$$q_i = q_{im} + \alpha \bullet s \qquad (7)$$

where the term α is the constant to make the charge linear, which should be -1 if the depleted charge in GaN layer and the substrate charge are ignored in the model.

According to the standard drift-diffusion current model and the definition of surface potential, the drain current is given as:

$$I_{ds} = \mu W C_{ox}\left(q_i \frac{a\varphi_s}{dy} - \phi_t \frac{aq_i}{dy}\right) \qquad (8)$$

With (7), (8) becomes:

$$I_{ds} = \mu W C_{ox}\left(q_{im} + \alpha \bullet s - \alpha \bullet \phi_t\right)\frac{ds}{dy} \qquad (9)$$

Based on the scattering mechanism, the channel electron mobility is affected by the gate voltage. An effective vertical electric model is useful in this study following the silicon based modelling method [21]. Moreover, when the drain voltage $V_{ds}$ is larger than the saturation voltage $V_{dsat}$ which is a possible operation bias for HEMT devices, the channel length modulation effect should be included carefully. To consider this effect, the $V_{dsat}$ will be modeled first and the length of saturation region will be given based on the solution of $V_{dsat}$.

To verify the core model with the saturation voltage, the TCAD simulations are performed with constant mobility and high field saturation model activated. The Fermi statistics is adopted in the TCAD setup and the Poisson equation and current continuity equations for electrons and holes are solved. As shown in Fig.5 (a), the blue dashed lines verify the core model by the core part simulation, and the red solid lines verify the model with internal nodes to incorporate the access region resistances. The saturation voltage feature is also verified by the model. As shown in Fig.5(b), the transfer characteristics reflect that the model can also capture the features in the sub-threshold region.

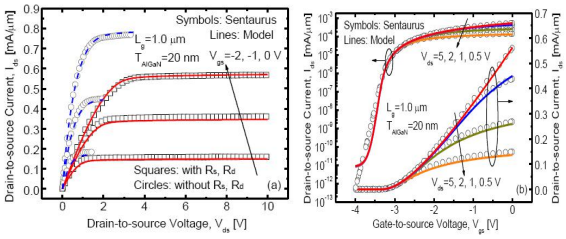


Fig.5 Comparison between the model and TCAD simulations for (a) output characteristics and (b) transfer characteristics.

In the model simulation, the self-heating effect is included with a thermal network feedback to the current model. This feedback is realized by iteration and the balance condition is that the drain current and channel temperature reach stable values which mean that the generated and dissipated heat achieves a balance. Fig.6 compares the model prediction with the measurements. The agreements for pulsed IV measurements at both T=125ºC and T=25ºC verify that the model can predict "how the temperature affects the current performance" correctly. Then, the agreements for the DC I-V measurements verify the correctness of the model calculation for "how the channel temperature changes during operation".

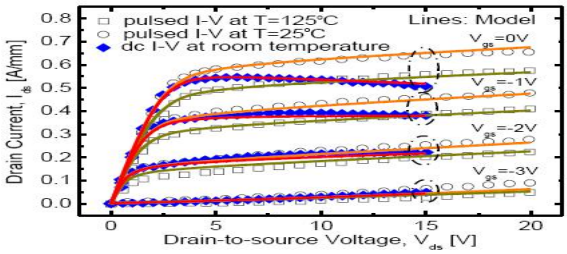


Fig.6 Comparison to verify the self-heating effect between the model and the puslsed and dc measurements at different temperature.

In this model, no detailed temperature-dependent thermal capacitance model is given. In some sense, even the thermal capacitance can be given as a fitting parameter, the model will not be that powerful for transient simulations considering the duty-cycle-dependent self-heating effect.

## 3 RESULTS AND DISCUSSION

The devices required for the model development were fabricated in PKU Lab., and the cross-sectional schematic of the device structure is shown in Fig.1. The heterostructure of the fabricated device consists of a 21nm $Al_{0.25}Ga_{0.75}N$ barrier and a 3.8μm GaN buffer layer grown on a p-type 500μm Si (111) substrate. Source/drain ohmic contacts were formed with e-beam evaporation of Ti/Al/Ni/Au metal stack and liftoff followed by rapid thermal annealing. The width of the devices is W=10μm. The T-shape gate features a 0.5μm extension to both sides on top of SiNx and typical gate footprints between 1μm and 5μm. The gate-source distance $L_{GS}$ is 1μm and the gate-drain distance $L_{GD}$ has typical values from 5, 10 to 15μm.

In this study, the model verifications by the fabricated device with $L_g$=1μm, $L_{GS}$=1.5μm and $L_{GD}$=5.5μm are demonstrated as the example. Fig.7 shows the comparison of the model-predicted transfer and output drain currents against DC I-V measurements. The curve cross in the transfer characteristics is due to the self-heating effect which is also shown in the output currents at high gate and drain biases. As shown in Fig.7 (a) in the sub-threshold region, the DIBL effect is not serious since this is a long channel device, but it can still be captured by the fitting parameters in the model.

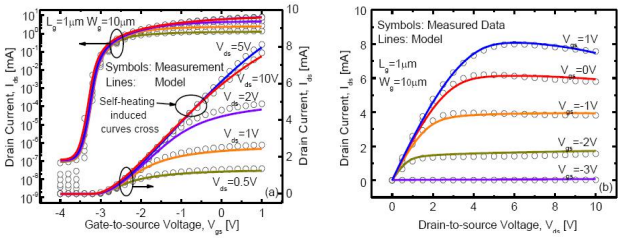


Fig.7 Comparison of (a) transfer and (b) output currents between the model and DC I-V measurements.

Fig.8 shows the comparison of the compact model-predicted transconductance and output conductance against the DC I-V measurements. The transconductance is highly non-linear because of the velocity reduction in the channel due to carrier scattering. The output conductance in the saturation regions is negative due to the self-heating effect, and this is also captured by the model.

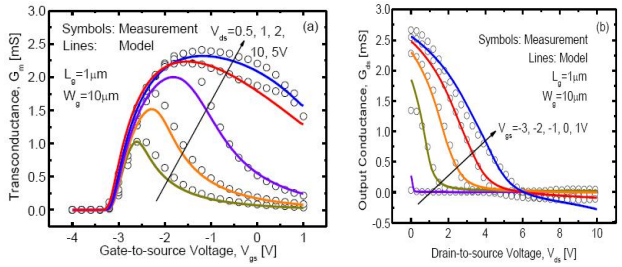


Fig.8 Comparison of (a) transconductance and (b) output conductance between the model and DC I-V measurements.

## 4 CONCLUSIONS

In this paper, a complete surface potential based DC I-V model for the GaN HEMTs has been developed. Both the surface potential calculation and I-V characteristics are included consistently. Some features like the channel length modulation effect and the self-heating effect are incorporated in the model, and the geometry dependence of RC thermal network is provided to capture the dynamic heating effect. The full model captures the main physics of GaN HEMTs, and is evaluated by both TCAD simulations and experimental measurements.

**Acknowledgement**

This work is funded by National Natural Science Foundation of China under Grants (61574005), by Fundamental Research Project of Shenzhen Sci. & Tech. Fund (JCYJ20160329161334453, JCYJ20170307164247428, JCYJ20170307164201104, JCYJ20170307172513653, JCYJ20170412153729436, JCYJ20170412153812353, JCYJ20170412153845293), and also by Guangdong Province SNSFC Fund (2018A030313973).

**References**

[1] R. T. Kemerley, and M. N. Yoder, Proceedings of the IEEE, vol. 90, pp. 1059–1064, June 2002.
[2] R. J. Trew, Proceedings of the IEEE, vol. 90, pp. 1032–1047, June 2002.
[3] M. A. Briere, International Rectifier, Dec. 30, 2008.
[4] Renee Yawger, Comp. Semiconductor, Feb. 19, 2014.
[5] I. Angelov, K. Andersson, D. Schreurs, D. Xiao, N. Rorsman, V. Desmaris, M. Sudow, and H. Zirath, Proceedings of Asia-Pacific Microwave Conference, Yokohama, Japan, 2006. pp. 279–282.
[6] Y. Tajima, Proceedings of Workshop 38th European Microwave Conference, Amsterdam, Netherlands, 2008.
[7] W. R. Curtice and M. Ettenberg., IEEE Trans. Microwave Theory and Tech., vol. 33, no. 12, pp. 1383-1393, Dec. 1985.
[8] J. D. Albrecht, P. P. Ruden, ect., IEEE Trans. Electron Devices, vol. 47, no. 11, pp. 2031–2036, Nov. 2000.
[9] M. A. Huque, S. A. Eliza, T. Rahman, H. f. Huq, and S. K. Islam, Solid-State Electronics, vol. 53, no. 3, pp. 341–348, Mar. 2009.
[10] P. Gangwani, S. Pandey, S. Haldar, M. Gupta,, Solid-State Electronics, vol. 51, no. 1, pp. 130-135, Jan. 2007.
[11] M. Li and Y. Wang, IEEE Trans. Electron Devices, vol. 55, no. 1, pp. 261–267, Jan. 2008.
[12] X. Cheng, M. Li, and Y. Wang, IEEE Trans. Electron Devices, vol. 56, no. 12, pp. 2881–2887, Dec. 2009.
[13] X. Cheng and Y. Wang, IEEE Trans. Electron Devices, vol. 58, no. 2, pp. 448–454, Feb. 2011.
[14] S. Khandelwal, Y. S. Chauhan, IEEE Trans. Electron Devices, vol. 59, no. 10, pp. 2856–2860, Oct. 2012.
[15] S. Khandelwal, C. Yadav, IEEE Trans. Electron Devices, vol. 60, no. 10, pp. 3216–3222, Oct. 2013.
[16] U. Radhakrishna, L. Wei, D. S. Lee, T. Palacios, and D. Antoniadis, IEDM Tech. Dig., pp. 319-322, Dec. 2012.
[17] W. S. Lau, J. B. H. Tan, and B. P. Singh, Microelectronics Reliability, vol. 49, no. 5, pp. 558-561, May 2009.
[18] Rashmi, A. Kranti, S. Haldar, and R.S. Gupta, Solid-State Electron., vol. 46, pp. 621–630, 2002.
[19] Jin He, Mansun Chan, Xing Zhang, Yangyuan Wang, IEEE Transactions on Electron Devices, TED-53, No.9, pp.2008-2016, Sept., 2006.
[20] TCAD Sentaurus device manual, Synopsys, Inc., Mountain View, CA, USA, Mar. 2010.
[21] G. Gildenblat, Compact modeling: principles, techniques and applications, New York: Springer Verlag, pp. 438–440, 2010.